Transconformations of the SERCA1 Ca-ATPase: A Normal Mode Study

Nathalie Reuter,* Konrad Hinsen,[†] and Jean-Jacques Lacapère*

*U410 INSERM. Faculté de médecine Xavier Bichat, Paris Cédex 18, France; and [†]UPR 4301 CNRS, Centre de Biophysique Moléculaire, Orléans Cédex 2, France

ABSTRACT   The transport of Ca^{2+} by Ca-ATPase across the sarcoplasmic reticulum membrane is accompanied by several transconformations of the protein. Relying on the already established functional importance of low-frequency modes in dynamics of proteins, we report here a normal mode analysis of the Ca^{2+}-ATPase based on the crystallographic structures of the $E1Ca_2$ and E2TG forms. The lowest-frequency modes reveal that the N and A(+Nter) domains undergo the largest amplitude movements. The dynamical domain analysis performed with the DomainFinder program suggests that they behave as rigid bodies, unlike the highly flexible P domain. We highlight two types of movements of the transmembrane helices: i), a concerted movement around an axis perpendicular to the membrane which "twists open" the lumenal side of the protein and ii), an individual translational and rotational mobility which is of lower amplitude for the helices hosting the calcium binding sites. Among all modes calculated for E1Ca, only three are enough to describe the transition to E2TG; the associated movements involve almost exclusively the A and N domains, reflecting the closure of the cytoplasmic headpiece and high displacement of the L7-8 lumenal loop. Subsequently, we discuss the potential contribution of the remaining low-frequency normal modes to the transconformations occurring within the overall calcium transport cycle.

INTRODUCTION

The P-type ATPases are a large family of membrane proteins that actively transport cations across biological membranes (Møller et al., 1996) to regulate ion concentrations in animal, plant, and yeast cells. The hydrolysis of ATP provides the required energy to move cations against their electrochemical potential gradient. The formation of a stable aspartyl-phosphoryl-enzyme intermediate distinguishes the P-type ATPases from the other ATPases such as the F- and V-type ATPases which are ATP synthases.

The calcium ATPase (Ca-ATPase) from skeletal muscle sarcoplasmic reticulum (SR) is structurally and functionally the best-studied active ion transporter (for reviews see Lee and East, 2001; Stokes and Green, 2003). It pumps the cytosolic calcium into the sarcoplasmic reticulum lumen. Two calcium ions per ATP molecule hydrolyzed are transferred from the cytoplasmic to the lumenal side while two (Yu et al., 1993) or three (Forge et al., 1993a; b) protons are counter-transported. The reaction cycle can be represented as in Fig. 1, where also the available atomic structural data are given. Since 1993 cryoelectron microscopy (cryoEM) has provided three-dimensional low-resolution structures of an $E2H_3$-P-like form of the SR Ca-ATPase in the presence of vanadate (Toyoshima et al., 1993; Xu et al., 2002; Zhang et al., 1998). More recently the release of the first atomic structure (Toyoshima et al., 2000) obtained from x-ray diffraction and corresponding to the $E1Ca_2$ form of the protein (Fig. 1), provided new structural information that could be linked with the numerous functional data. It has confirmed most of the structural features anticipated by early

secondary structure predictions (Green and Stokes, 1992; Stokes and Green, 2000). The Ca-ATPase is made up of three cytoplasmic domains, named actuator (A), nucleotidic (N), and phosphorylation (P), 10 transmembrane helices (M1–M10: M domain), and loops of various lengths (Fig. 1). The x-ray and cryoEM-derived structures have given a snapshot of different intermediates and their comparison has suggested cytoplasmic domain movements. The release of a second atomic structure of the Ca-ATPase (Toyoshima and Nomura, 2002) ($E2H_3$-TG form in Fig. 1) has provided new insights into the transconformation mechanisms. Indeed, unlike the $E1Ca_2$ conformation which is opened, the $E2H_3$-TG form shows a much higher proximity of the cytoplasmic domains, which can be described as a closure of the cytoplasmic headpiece. The calcium binding sites lie in the transmembrane section of the protein, between helices M4, M5, M6, and M8. The comparison of the two atomic structures with and without calcium ($E1Ca_2$ and $E2H_3$-TG) shows large movements in the transmembrane region and suggests access routes for the calcium ions. However, there exist more than two stable conformations of this protein and the molecular interactions that trigger these transitions are not well understood. In the present study our goal was to investigate the dynamics of the transconformations using molecular modeling. Indeed, this approach provides several powerful tools for computing the dynamics of proteins. Molecular dynamics (MD) is perhaps the most widely used technique, but given the number of atoms (~15,000 with hydrogen atoms for the Ca-ATPase) and the time scale of the reaction cycle (several milliseconds), MD simulations of the Ca-ATPase with a meaningful simulation time is currently difficult. One alternative is to simplify the system by studying only a part of interest. Costa et al. (Costa and Carloni, 2003) performed MD simulations of the M and P domains of the Ca-ATPase. This study provides interesting
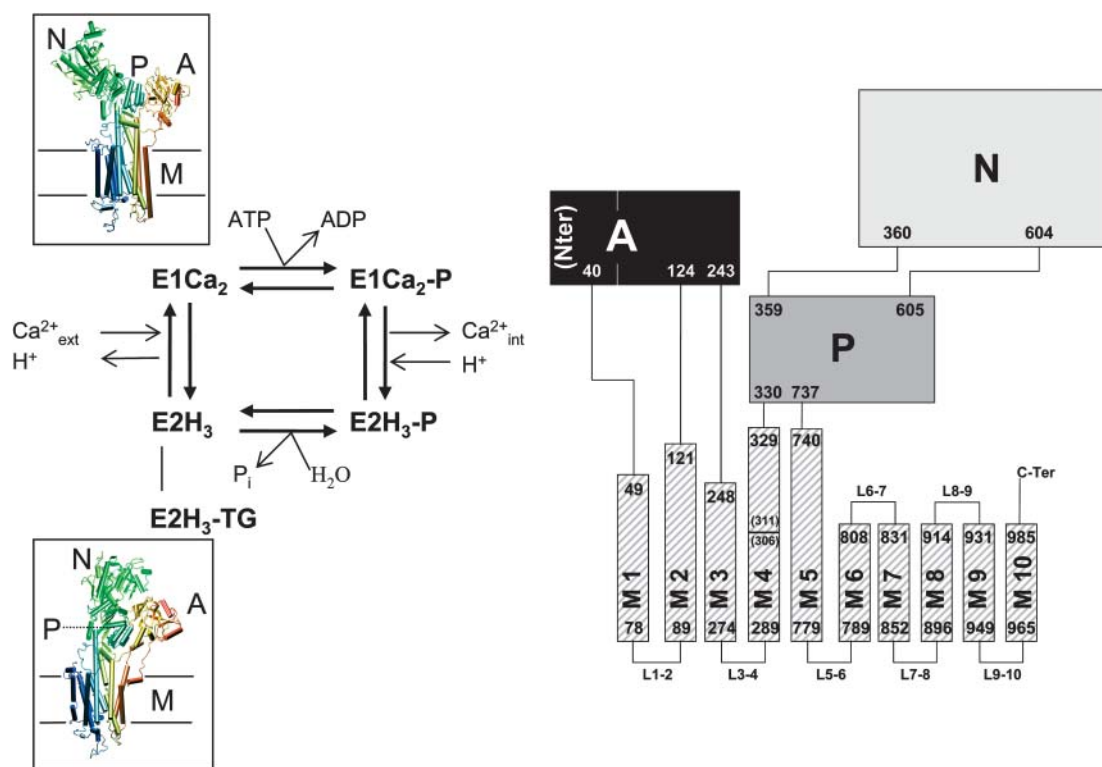
FIGURE 1 Topological domains (*right*) and reaction cycle (*left*) of the Ca-ATPase with known atomic structures. The definition of the cytoplasmic domains (Nter, A, P, and N for N-terminal, actuator, phosphorylation, and nucleotide, respectively) is based on the crystal structure (1eul) of the $E1Ca_2$ form (Toyoshima et al., 2000). The definition of the 10 transmembrane helices (M1–M10) has been determined by the STRIDE program (Frishman and Argos, 1995), implemented in the VMD visualization tool (Humphrey et al., 1996). The frontier residues are represented by their numbers in the sequence of the calcium pump. A scheme describing the minimal number of intermediates is presented on the left with the known atomic structures (1eul and 1iwo corresponding to $E1Ca_2$ and E2TG forms, respectively).

insights into the calcium-binding mechanism, since they suggest that the two ions reach their binding sites via two specific pathways. Normal mode analysis (NMA) is a better suited approach than molecular dynamics for the whole Ca-ATPase since it is much less computer demanding. Several tools based on NMA have been developed (Bahar et al., 1997; Brooks et al., 1983; Go et al., 1983; Hinsen, 1998; Hinsen et al., 2000; Hinsen et al., 1999; Levitt et al., 1985; Li and Cui, 2002; Marques and Sanejouand, 1995; Mouawad and Perahia, 1993; Schulz, 1991; Tama et al., 2000; Tirion, 1996) and successfully applied to predict the collective, large amplitude motions of several macromolecules (for reviews see refs. Cornell and Louise-May, 1998; Hayward, 2001). These methods are based on the hypothesis that the vibrational normal modes exhibiting the lowest frequencies (also named soft modes) describe the largest movements in a protein and are the ones functionally relevant. An NMA study involving all atoms of the Ca-ATPase has been recently reported by Li et al. (Li and Cui, 2002). This work describes the structural flexibility of the cytoplasmic domains (especially N), identifies hinge regions (A/M and N/P interfaces), and reports correlated motions between cyto-

plasmic and transmembrane domains. We previously reported (Reuter et al., 2003a,b) similar features of flexibility and correlated motions of different domains in the $E1Ca_2$ form of the Ca-ATPase using NMA with a simplified potential based on $C\alpha$ atoms (Hinsen et al., 2000).

In the present study, we have calculated the whole set of modes; we first present a thorough analysis of the 10 lowest frequency modes of the $E1Ca_2$ form and characterize them with respect to the regions of the protein most displaced in each mode. Second, we illustrate the flexibility of the protein by a residue-based deformation energy analysis enabling the characterization of Ca-ATPase regions that can be considered as rigid bodies. Third, we highlight two types of motions for the transmembrane helices: i), a correlated twist of the 10 M helices and ii), independent rotations and translations of each M helix. Finally, we identify the few normal modes involved in the difference between the two known atomic structures of the Ca-ATPase ($E1Ca_2$ and $E2H_3$-TG forms). Consequently, we discuss the potential contribution of the remaining low-frequency normal modes to the transconformations occurring within the overall calcium transport cycle.

MATERIAL AND METHODS

Atomic structures

The atomic coordinates of the E1Ca$_2$ and E2TG forms of the Ca-ATPase were extracted from the x-ray structures referenced 1eul (Toyoshima et al., 2000) and 1iwo (chain A) (Toyoshima and Nomura, 2002) in the Protein Data Bank (Abola et al., 1987; Bernstein et al., 1977), respectively. The secondary structure elements (helices and extended conformations) were calculated with the program STRIDE (Frishman and Argos, 1995). For the normal modes calculation, we used a simplified model consisting of only the Cα atoms (994) of the protein, prepared from the 1eul atomic structure.

Normal mode calculations

A normal mode analysis consists of the diagonalization of the matrix of the second derivatives of the energy with respect to the displacements of the atoms, in mass-weighted coordinates (Hessian matrix). The eigenvectors of the Hessian matrix are the normal modes, and its eigenvalues are the squares of the associated frequencies. The low-frequency normal modes are believed to be the ones functionally important. To perform a NMA on the E1Ca form of the pump, we used the approximate normal analysis method developed by Hinsen (Hinsen, 1998), which represents very well low-frequency domain motions at negligible computational cost. The force field used is slightly different from the one used in the original publication and has been described in reference (Hinsen et al., 2000). It uses only the Cα atoms of the protein, which however are assigned the masses of the whole residues they represent.

Briefly, the functional form of the force field is

$$U(\mathbf{R}_1, \ldots, \mathbf{R}_N) = \sum_{\text{all pairs i,j}} V(\mathbf{R}_i - \mathbf{R}_j). \qquad (1)$$

$V(\mathbf{r})$ is the harmonic pair potential describing the interaction between the Cα atoms:

$$V(\mathbf{r}) = k(|\mathbf{R}_{ij}^{(0)}|)(|\mathbf{r}| - (\mathbf{R}_{ij}^0|)^2, \qquad (2)$$

where $\mathbf{R}_{ij}^{(0)}$ is the pair distance vector, $(\mathbf{R}_i - \mathbf{R}_j)$ is the input configuration, and k is the pair force constant:

$$k(r) = \begin{cases} 8.6 \times 10^5 \, \text{kJ} \, \text{mol}^{-1} \, \text{nm}^{-3} \\ \times r - 2.39 \times 10^5 \, \text{kJ} \, \text{mol}^{-1} \, \text{nm}^{-2} & \text{for } r < 0.4 \, \text{nm} . \\ 128 \, \text{kJ} \, \text{nm}^4 \, \text{mol}^{-1} \times r^{-6} & \text{for } r \geq 0.4 \, \text{nm} \end{cases} \qquad (3)$$

The NMA tools are implemented in the Molecular Modeling Toolkit (MMTK) (Hinsen, 2000), which is also interfaced with the VMD program (Humphrey et al., 1996) to help the visualization. All modes were calculated, i.e., three times the number of Cα atoms ($3 \times 994 = 2982$) in a relatively short time; the calculation took ~30 min on a 1.2-GHz Athlon processor with 1 GB memory. The first six modes (zero-frequency modes) correspond to global rotation and translation of the Ca-ATPase and will be ignored in the following analysis. The lowest frequency mode of interest is thus mode number 7.

Atomic displacement

Normalized squared atomic displacements (D_i) for each Cα atom ($i = 1–994$) are calculated as follows:

$$D_i = \mathbf{d}_i^2 \bigg/ \left(\sum_{j=1}^{994} \mathbf{d}_j^2 \right), \qquad (4)$$

where $\mathbf{d}_i$ is the component of the eigenvector corresponding to the ith Cα.

Vector field

A vector field representation was calculated as described by Thomas et al. (Thomas et al., 1999). The vector field is calculated over cubic regions with an edge length of 3 Å, containing on average 1.3 Cα atoms. The vector field defined on a regular lattice at the center of each cube is the mass-weighted average of the displacements of the atoms in the cube.

Deformation analysis and definition of the dynamical domains

The DomainFinder program (Hinsen et al., 1999) allows the determination of dynamical domains of proteins. A dynamical domain of a protein is a relatively rigid region, moving as a rigid body, that is separated from the other domains by more flexible inter-domain regions. The other definition of domains in a protein derives from the structural aspects of the molecule; a structural domain of a protein is a compactly folded part linked to other domains by only a few peptide chains. This is for example the case of the nucleotidic domain in the Ca-ATPase (see Fig. 1). Determination of dynamical domains, based on normal modes, is an effective tool for characterizing the flexibility of a complex protein. Briefly, starting from a predefined set of low-frequency normal modes (here modes 7–16) this program evaluates a deformation measure for each residue of the Ca-ATPase and consequently identifies rigid and nonrigid regions. The rigid regions are classified according to their global motion and the dynamical domains are composed of residues having the same rigid body motion. The coarseness, input parameter of the calculation, specifies how similar the rigid body motions of the different residues should be to consider that these residues form a dynamical domain; thus the smaller the coarseness, the finer the definition of the domains. Since the deformation energies of modes 7–16 range from 2 to 48, the deformation analysis based on these 10 modes was performed with a deformation threshold equal to 40. The dynamical domain decomposition was performed with different values of the coarseness parameter; 20 and 30 (Fig. 4) and 10, 15, 40, and 50 (data not shown).

Generation of structures along a normal vector and subsequent minimization

Structures displayed in Fig. 6 were generated by applying eigenvectors of mode number 9 to the Cα coordinates of the 1eul x-ray structure. The side chains were then copied from 1eul to the newly obtained Cα coordinates. This is done by superimposing triplets of consecutive Cα atoms of both structures and pasting the side chain of the central one. The procedure is repeated along the protein chain. Subsequent minimization of the side chains was performed with the MMTK package, using the steepest descent algorithm with the Amber94 force field (Cornell et al., 1995).

Overlap between a displacement vector and the normal modes

The calculation of the dot product (overlap) between a displacement vector and the full set of normal modes identifies which modes contribute most to the given displacement. By definition, the cumulative sum of the overlap squared is equal to one. The different displacement vectors are calculated as described below.

Movements of A and N domains

In an attempt to find a general framework for all movements we arbitrarily chose the same set of three axes for both domains. Previously reported movements of the cytoplasmic domains of the pump (Toyoshima and Nomura, 2002; Xu et al., 2002) have been mostly described with respect to the membrane plane (parallel or perpendicular displacements with respect to

it). As the membrane plane is difficult to define rigorously we calculated the three axes of inertia of the M region, which is a rigorous mathematical, and thus, reproducible way of defining axes to describe domain movements of the Ca-ATPase. We thus obtained one axis almost perpendicular to the membrane and two axes parallel to it, and used them to describe movements of A and N domains. Practically, these axes were calculated and translated so that their intersection coincides with the center of mass of the A domain (to describe A domain movements), or the N domain (to describe N domain movements). The translation vector of the domain along a given axis has a component for each $C\alpha$ atom of the domain which corresponds to a normalized vector, parallel to the axis. The components of the rotation vector for each $C\alpha$ atom of the domain are calculated as the cross-product of the axis with the vector between the atom and the center of mass. For each of these cytoplasmic domains, we could thus discuss in terms of rotational and translational movements parallel or perpendicular to the membrane.

Helix rotation and translation around its axis

The axis of an helix is defined as the principal axis of inertia of the $C\alpha$ atoms composing the helix (residues defined in Fig. 1, right). The components of the rotation vector on each $C\alpha$ atom are calculated exactly as for A and N domains (see above).

Overlap between the difference vector of the two x-ray structures and the normal modes

To identify which modes contribute most to the transition between the two structures, the strategy used is the same as described above for the overlap between a displacement vector and the set of modes, except that the displacement vector is here replaced by the difference vector between the two structures, which were superimposed beforehand.

RESULTS

The nature of the low-frequency normal modes

General considerations

Normal modes of the E1Ca$_2$ form of the Ca-ATPase are calculated as described in the Material and Methods section where the technical aspects of the methodology employed are also detailed. All modes are calculated and ranked from low to high frequencies. Absolute frequency values can not be determined accurately and therefore will not be discussed in a quantitative way. Amongst the 2982 modes obtained, we are essentially interested in the lowest frequency (or soft) modes.

Normalized squared atomic displacements and vector field representation

In an attempt to characterize the displacements associated with those normal modes, we first calculated, for each mode, the normalized squared atomic displacements, i.e., the square of the displacement of each $C\alpha$ atom, normalized so that the sum over the 994 $C\alpha$ atoms equals one. The normalized atomic displacements for modes 7–16 are represented in Fig. 2, as a function of the amino acid sequence. The highest peaks in the plots of Fig. 2 corresponds to the most displaced residues in the corresponding mode. The regions displaced in

each mode are also visualized using vector fields (Thomas et al., 1999) to represent the most important displacements associated with the various slow modes (Fig. 3). This allows us to characterize the modes depending on which region is the most displaced.

The first two modes, 7 and 8, involve mostly displacements of the N domain as a whole (Figs. 2 and 3, *a* and *b*). Mode 9 is more delocalized, it clearly displaces the N domain as a whole but also involves movements of lumenal loops (especially L1-2, L3-4, and L7-8) and most of the M helices (Fig. 2). Indeed, M5, M6, and L56 exhibit smaller displacements than the other loops and M helices. Peaks corresponding to transmembrane helices are always higher at the lumenal extremity of each helix. The corresponding movement is a torsion of the transmembrane region around an axis perpendicular to the membrane plane running through the middle of the Ca-ATPase (Fig. 3 *c*). The center of mass of each helix remains close to its initial position whereas the lumenal extremities and the connected loops undergo large displacements. The presence of movements of N domain, M helices, and lumenal loops in this mode 9 suggests that their displacements are correlated. Modes 10–12 describe correlated movements of the A domain and the N-terminal region (residues 1–40) (Fig. 2, *d–f*). This movement is more localized in mode 12 (Fig. 3 *d*). This coupling is in line with the usual description of this region as a domain; even if these two parts are separated in the sequence by the first two transmembrane helices, they appear to be displaced together. Moreover, the lumenal loop L7-8 exhibits movements correlated to movements of this domain without large displacement of the remaining parts of the protein (modes 10 and 11). Mode 13 involves displacements delocalized almost equally over all cytoplasmic domains (Figs. 2 *g* and 3 *e*). This mode shows coupled movements of A, P (only residues 622–700), and N domains, suggesting a cooperativity between these domains. Important displacements of the L7-8 loop are visible for modes 14 and 15 (Fig. 2, *h* and *i*). This long loop (almost 50 residues) shows either movements that are almost independent, as revealed by the especially prominent peak for mode 15, or correlated movements with the M helices (mode 9), and the N and A domains (modes 9–11, and 14). Modes 14 and 16 exhibit a high peak (Fig. 2, *h* and *j*) for residues Ser-504 to Ala-506 of the N domain which correspond to the first tryptic (T1) cleavage site (Arg-505). It suggests an intrinsic mobility of this T1-containing loop with respect to the N domain. This peak, especially pronounced for mode 16, is associated with peaks in the A domain, with the highest corresponding to the second tryptic (T2) cleavage site (Arg-198). This T2-associated peak is also visible in modes 10–13. Conversely to the T1 site, movements of this T2 site are always correlated with movements of the A domain as a whole (Fig. 2). The modes above 16 have very close frequencies and therefore, analysis of the associated displacements in an independent manner is meaningless.
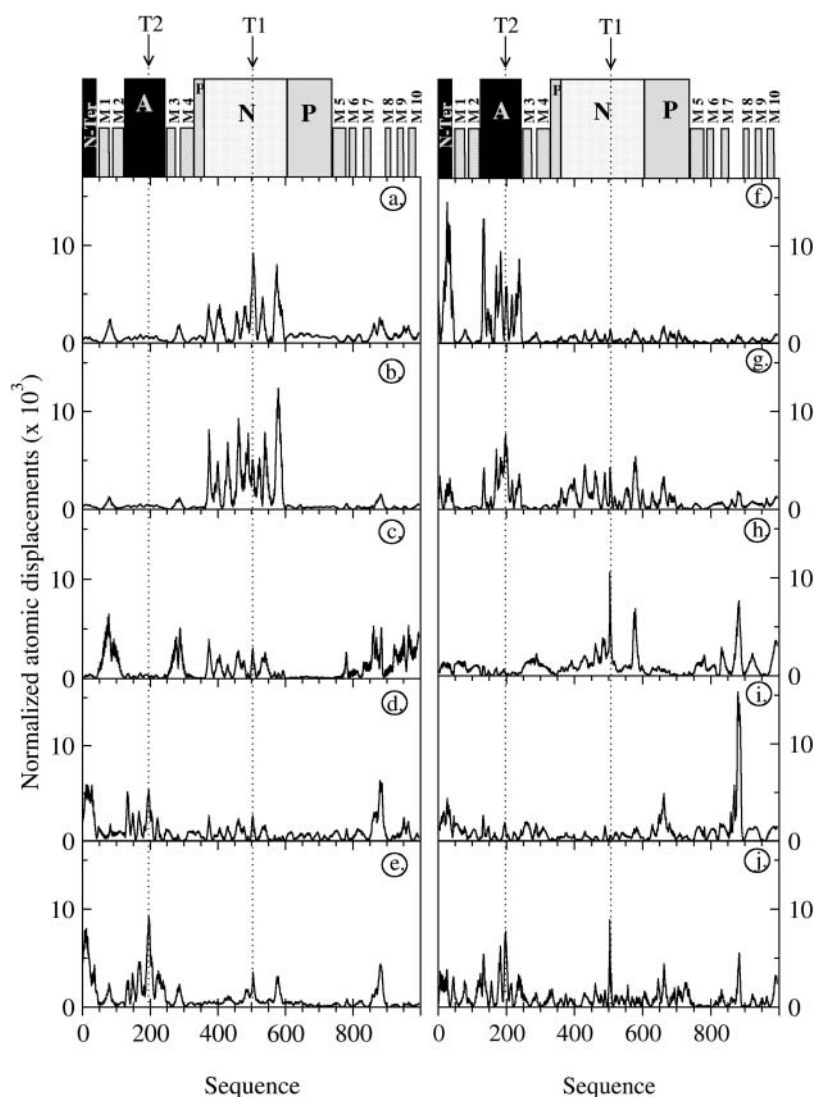
FIGURE 2 Normalized squared atomic displacement of the slowest modes of E1Ca$_2$ form. *a.* mode 7, *b.* mode 8, *c.* mode 9, *d.* mode 10, *e.* mode 11, *f.* mode 12, *g.* mode 13, *h.* mode 14, *i.* mode 15, *j.* mode 16. The atomic displacement is plotted versus the residue number in the sequence of the pump (from 1–994). Sketches above plots *a* and *f* highlight the correspondence between the regions (Nter, A, P, and N for N-terminal, actuator, phosphorylation, and nucleotide, respectively) defined in Fig. 1 and sequence numbers. Tryptic cleavage sites obtained by limited digestion (T1 and T2) are also shown on top of the plots and highlighted by dotted lines

Domain analysis (modes 7–16)

The deformation analysis of the E1Ca$_2$ form of the Ca-ATPase (Fig. 4 *a*) shows three important rigid regions which correspond roughly to N, A(+Nter) domains, and the transmembrane part of the M domain. Conversely, the P domain is more complex. A first part, comprising extended β-sheets (β2–β6) of the Rossman fold plus the helices P4 and P5 is rigid (residues L342–C349, I622–K629, N645–Y694, T698–M700, I716–A719; *red* in Fig. 4 *a*). A second part, made of the rest of the P domain and the upper part of M4 and M5 is more flexible (*green* and *blue* colored in Fig. 4 *a*). It is worth noting that the phosphorylation site (D351) is in the flexible region. Thus, unlike N and A(+Nter) domains, the topological P domain (Fig. 1) can not be considered as a rigid body. Several parts of the protein are identified as flexible, they correlate to previously described hinge regions of A(+Nter) and N motions (Lee and East, 2001; Li and Cui, 2002): i), connection between M helices

and A(+Nter) domain (residues P42–K47, K120–E125, and A240–D245) and ii), links of the P to the N domain (residues N-359, Q-360, R-604, and K-605) (*blue* colored in Fig. 4 *a*).

Performing a domain decomposition analysis with different values of the coarseness parameter confirms that P can not be regarded as a dynamical domain. Indeed, for well defined dynamical domains, changing the coarseness does not modify significantly its definition (Thomas et al., 1999). Fig. 4, *a–c* represents dynamical domains with different colors and shows that two domains (*green* and *red*) remain unchanged for different values of the coarseness parameter. They correspond to N and A(+Nter) domains in green and red, respectively. Changing the coarseness from 20 to 40 drastically modifies the domain definition of the central region of the Ca-ATPase. With a coarseness of 20 (Fig. 4 *b*), the central blue dynamical domain corresponds to the topological domain P (N330–N359 and K605–D737) augmented by the top part of helix M5 (from P to residue Y754) and part of the L6-7 loop (M817–P824), as well as
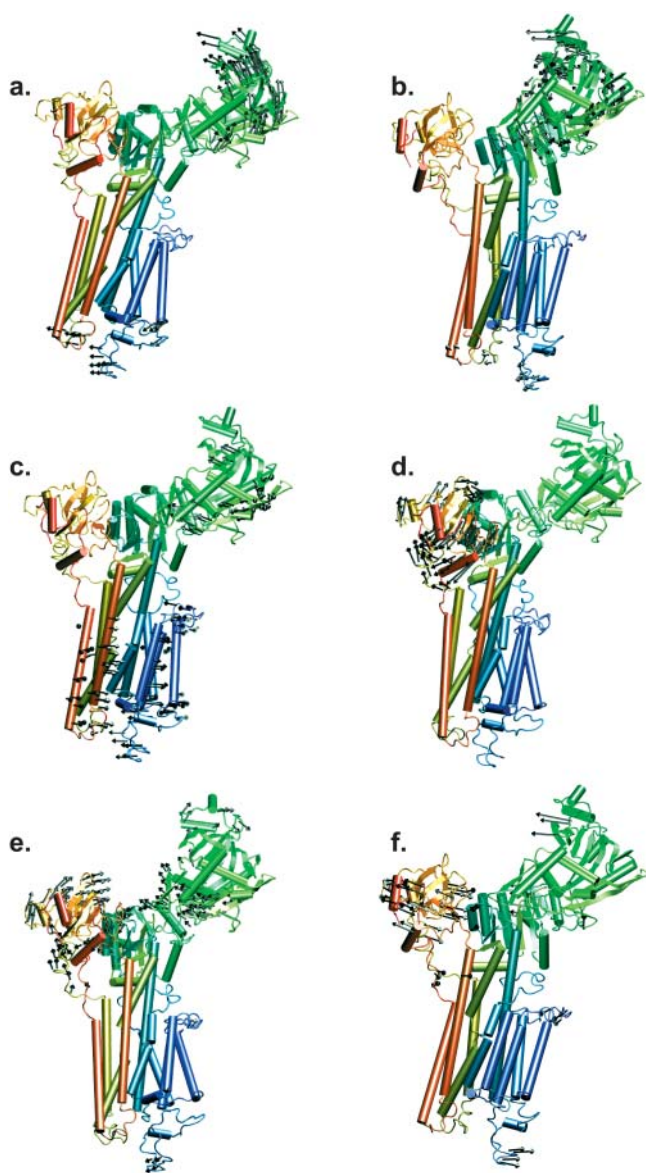
FIGURE 3 Vector field representation of the slowest modes of E1Ca$_2$ form. *a*. mode 7, *b*. mode 8, *c*. mode 9, *d*. mode 12, *e*. mode13, *f*. mode 16. For the sake of clarity, only vectors having a length greater than the average atomic displacement (calculated over all Cα atoms) for the mode considered are represented.

a few adjacent residues of N and A. With a higher coarseness (30), the size of the central dynamical domain increases and it now contains the stalk region and the top part of the transmembrane helices (colored in *cyan* in Fig. 4 *c*). Further increase of the coarseness parameter does not significantly change the domain decomposition, whereas reduction of the coarseness to values below 20 splits the Ca-ATPase into a collection of artificial regions with regards to topological and/or functional domains. Thus, whatever the coarseness value used we never observe a dynamical domain that coincides with the topological P domain; the P region is a flexible region and does not behave as a rigid body. This

correlates with data presented in Fig. 2 where no displacement of P as a whole can be observed. The transmembrane region can not be considered as a dynamical domain either. Indeed, the transmembrane residues belong to two different dynamical domains (colored *yellow* and *cyan* in Fig. 4, *b* and *c*). The boundary between these domains is parallel to the membrane plane and moves upwards when the coarseness increases. Even though this transmembrane part of the Ca-ATPase has been defined as a rigid region (Fig. 4 *a*) it is not a dynamical domain because it undergoes only small deformations (Figs. 2 and 3). Conversely, the topological N and A(+Nter) domains undergo large amplitude movements as rigid bodies. We therefore demonstrate that topological domains of the Ca-ATPase are not necessarily dynamical domains.

Domain movements

Analysis of both rotation and translation movements of the above defined dynamical domains (N and A(+Nter)) has been performed by measuring the contributions of the various low-frequency modes to the displacement along and around perpendicular axes (Fig. 5, *left*). These contributions (square of the dot products) are plotted against mode numbers in Fig. 5 (*right*).

The analysis of the individual low-frequency modes has shown that several modes (10, 11, 12, 13, and 16) contribute to displacements of the A domain (Figs. 2 and 3). As expected, these modes are observed to contribute the most to the rotation (and translation) of A around (and along) the chosen axes; the highest peaks are found for modes 11, 12, 13, and 16. Interestingly, one can distinguish translation- and rotation-type modes, illustrating that not all modes are contributing equally to these movements. Fig. 5 shows that modes 12 and 13 contribute most to the rotation around an axis parallel to the membrane (axis 1) whereas mode 16 has the highest contribution to rotation around the axis perpendicular to the membrane (axis 2). Fig. 5 also shows that mode 11 contributes most to the translation along the axis perpendicular to the membrane (axis 2). For the N domain, the same analysis is more difficult since several modes contribute equally to the three axes of both rotation and translation. Mode 8 contributes to rotation along the three axes and more than the others to the rotation around an axis parallel to the membrane (axis 3). Mode 14 contributes most to translation along the axis perpendicular to the membrane (axis 2). Since absolute frequencies are not determined accurately, amplitudes of both translational and rotational movements can not be quantified and thus compared. However, the modes having a high contribution in rotation along the three axes defined for N have lower frequencies than the ones having a high contribution in translation. This lets us suppose that rotationlike movements of N should be of higher amplitude than translations. Modes contributing to
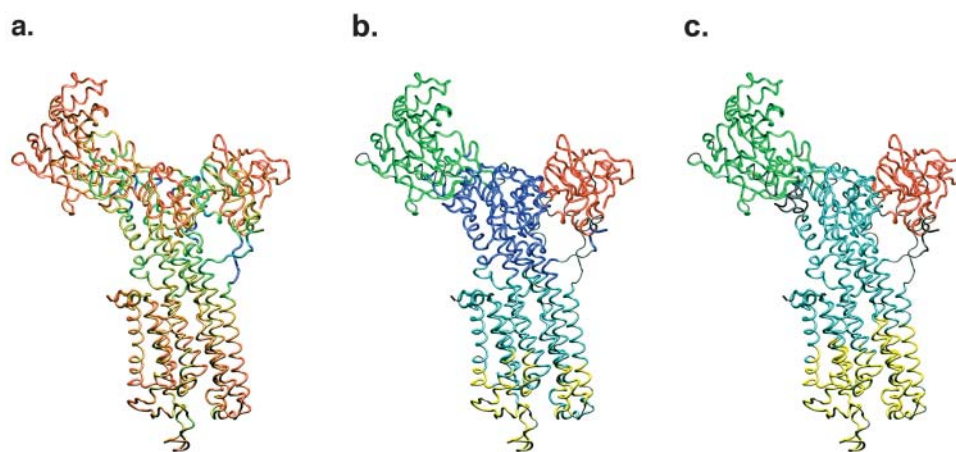
FIGURE 4 Deformation analysis (*a*) and domain decomposition of E1Ca$_2$ form, with increasing coarseness values of 20 (*b*) and 30 (*c*). The most rigid regions (small deformation energy) are represented in red on the deformation energy picture and blue is used for the most flexible parts. Green corresponds to regions for which the deformation energy is close to the deformation threshold. Red and green regions are candidates for dynamical domains. In *a*, *b*, and *c*, the stable domains are represented in red and green. The definition of the blue, cyan, and yellow domains varies with the value of the coarseness.

rotation and translation of A(+Nter) have close frequencies, so no conclusion can be made on their relative amplitude.

Displacements of the helices

Ca transport by the Ca-ATPase occurs through several steps including Ca entry from the cytoplasmic side to reach calcium binding sites and release to the lumenal side. The atomic structure (1eul) clearly describes the membranous calcium binding sites, but there is no obvious channel leading either from the cytoplasm to these site or from these sites to the lumenal side (Lee and East, 2001; Toyoshima et al., 2000; Toyoshima and Nomura, 2002). Thus, there have to be movements of the helices in the TM region to generate pathways for the entry or the release of the ions. Molecular dynamic simulations of the Ca-ATPase in its different calcium bound and free forms suggest that the two ions reach their specific binding sites I and II via two different pathways (Costa and Carloni, 2003). Normal mode analysis of the calcium-bound form suggests twisting motions of the M helices, which could be involved in the opening mechanism toward the lumen (Li and Cui, 2002). In a preliminary study we reported, using a similar approach, that the transmembrane segments undergo significant displacements (Reuter et al., 2003a,b). In the present article, we characterize two types of displacements: individual and concerted movements

of M helices. First, as Figs. 2 and 3 show that only the low-frequency mode 9 clearly exhibits large concerted movements of the 10 helices, we investigate the structural modifications induced by this mode. Then, since it is expected that the helices undergo smaller movements than the cytoplasmic domains, the mobility of each transmembrane helix is investigated in the whole set of modes (2982).

Concerted movements

Analysis of rotations of the M domain, performed as described above for the A and N domains, shows that mode 9 accounts for 30% of the rotation of the domain around its principal axis of inertia, i.e., quasi-perpendicular to the membrane. None of the other modes contributes more than 5%. Fig. 6 shows the two conformations of the Ca-ATPase obtained by following the eigenvector of mode 9, in both directions starting from the E1Ca$_2$ conformation (see Material and Methods section). To highlight the most significant displacements, we present two different superpositions of the two structures. The first one (Fig. 6, *a* and *b*) superimposes the two sets of coordinates by minimizing the RMS deviation (RMSD) of the A and P regions which exhibit low atomic displacement (Fig. 2 *c*). The second one (Fig. 6 *c*) superimposes the M helices by minimizing the RMSD of the residues.
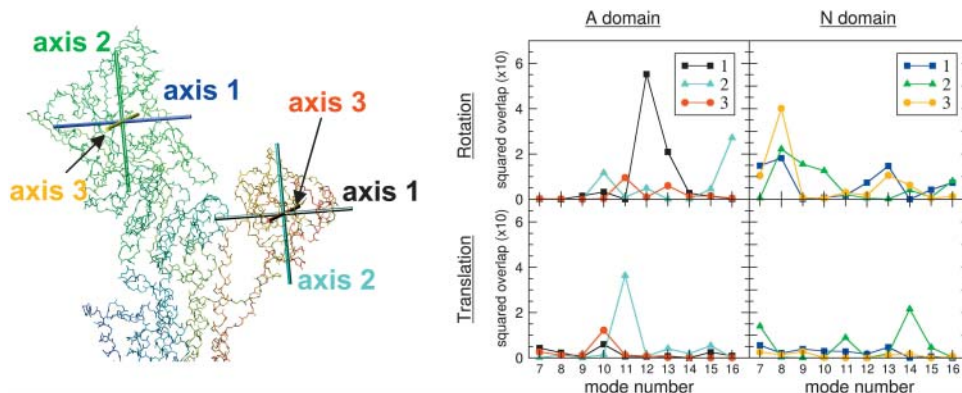

FIGURE 5 Movements of cytoplasmic domains of E1Ca$_2$ form. (*Left*) Orthogonal axis used to characterize the movements and (*right*) squared overlap (×10) between the modes and the displacement vectors.
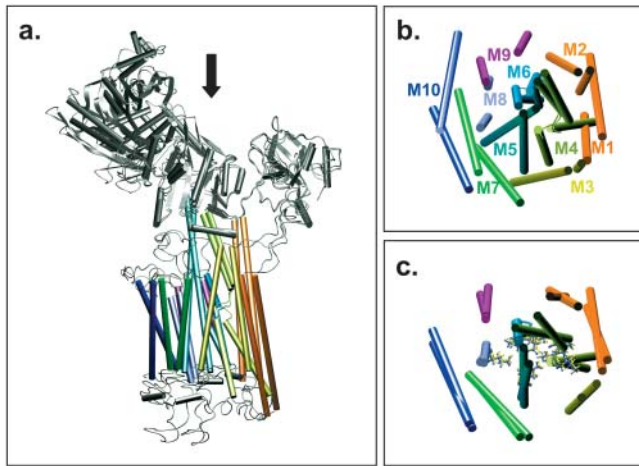
FIGURE 6 Conformations generated along the eigenvector of mode 9 of E1Ca$_2$ form. *a.* A side view (parallel to the membrane) of the whole protein is displayed, the two structures generated following the eigenvector of mode 9 have been superimposed by minimizing the RMSD of the A and P regions (RMS A and P: 1.48Å, RMS all: 8.38 Å). *b* and *c*, top view of the transmembrane region (along the arrow shown in *a*) obtained by superimposing either the A and P regions (*b*) or the M1–M10 helices (*c*) (RMS helices: 2.32 Å, RMS all: 17.12 Å). Side chain of the amino acids (V304, A305, I307, and E309 of M4; N768 and E771 of M5; N796, T799, and D800 of M6, E908 of M8) involved in the calcium binding sites are displayed in balls and sticks in *c*.

The protein undergoes a torsion-type movement around an axis perpendicular to the membrane plane (Fig. 6). The helices are rotated in one direction whereas the N domain is moved in the other direction (Fig. 3 *c*). The helices are significantly displaced with respect to the A and P regions (Fig. 6 *b*) but they are displaced in a concerted way. Indeed, the M region can be superimposed with a fairly low RMSD (2.32 Å) meaning that the relative positions of the helices are well conserved (Fig. 6 *c*). In particular, the geometry of the calcium binding sites does not change significantly (ball and sticks in Fig. 6 *c*). Indeed, the Cα atoms of the amino acids involved in site I and site II (V304, A305, I307, E309, N768, E771, N796, T799, D800, E908) can be very well superimposed. Conversely, lumenal extremities of the M helices are displaced (Fig. 2 *c*). The global motion is a twist of the M helices opening the lumenal side of the bundle made of the 10 helices. Such a mechanism may suggest a possible exit for the calcium bound. Moreover, the correlated rotation of the N domain in the opposite direction might also suggest a coupled mechanism occurring in the ATP dependent calcium transport.

Individual movements

For each helix (M1–M10), we define its principal axis of inertia (see Material and Methods section) and the rotation (or translation) vector of the Cα atoms of this helix around (or along) the axis. The cumulative squared overlap between the modes and the rotation or translation is plotted versus

mode numbers in Figs. 7, *a* and *b*, respectively. One can not distinguish particular modes contributing significantly more than the others, neither for rotation nor for translation. Seventy percent of both the rotation (Fig. 7 *a*) and translation (Fig. 7 *b*) of each of the helices is described by the first third of the set of normal modes (1000 out of 2982) i.e., low-frequency modes, which certainly means a functional role of this type of displacement of the helices. The main contribution to the displacements is found for modes higher in frequency than the modes describing the displacements of the cytoplasmic domains. In fact, 70% of the translation and rotation of the A and N domains could be described by the first 30 modes, whereas only 10% of the translation and rotation of the helices is observed for 100 modes. This means that the rotation and translation of each helix are of smaller amplitude than the movements of the N and A domains. This was expected since the packed environment of the TM region and also the hydrogen bond network in the hydrophobic core should not allow large displacement of the helices.

A comparison of Fig. 7, *a* and *b*, shows that rotations of the helices are of smaller amplitude than their translations since the modes contributing the most to the translations are of lower frequency than those describing the rotations. 150 modes are enough to describe 70% of the translation of M1 and 600 modes account for 70% of the translation of M8, the other helices being within this range. Conversely, 250 modes are needed to describe the rotation for helix M3 and 950
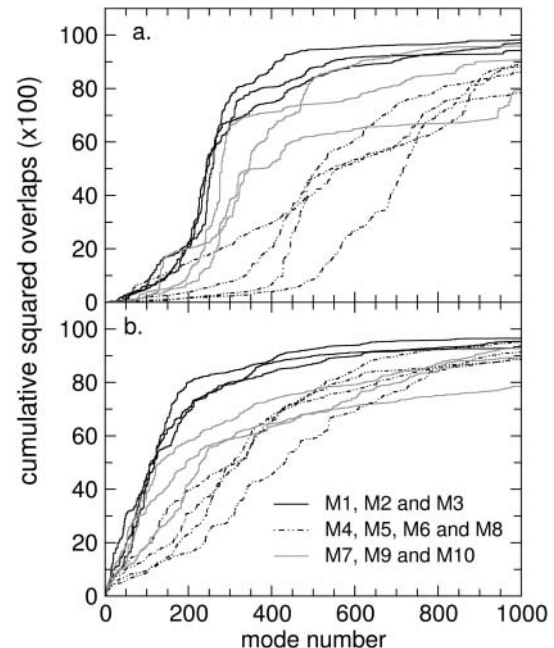

FIGURE 7 Cumulative summation of the squared overlap between the normal modes and the normalized rotation (*a*) and translation (*b*) vectors defined on the Cα atoms of each helix of the E1Ca$_2$ form (1eul). The cumulative squared overlaps ($\times$100) are plotted against mode numbers (*x* axis restricted to modes 7–1000). Solid lines represent helices M1, M2, and M3, dashed lines helices M4, M5, M6, and M8, dotted lines helices M7, M9, and M10.

modes for M7. More interesting is the difference between helices participating in the ion binding sites (M4, M5, M6, and M8) and the other ones. This is highlighted by the fact that the rotation of helices M1, M2, M3, M7, M9, and M10 is described by slower modes (50% reached with modes number 240–340) than helices M4, M5, M6, and M8 (50% reached with modes 500–720). This is also true for the translation but to a lesser extent. This means that helices hosting the binding sites undergo smaller amplitude displacements than the other ones. Among them one can also differentiate helices M1–M3 which have higher amplitudes of displacement than the other ones (M7, M9, and M10). They are connected to the A(+Nter) domain (Fig. 1) and located on the same side of the Ca-ATPase (Fig. 5). Since this cytoplasmic domain undergoes large amplitude movements, it could explain the higher mobility of the connected helices.

Which normal modes are involved in the transition between the calcium-bound (E1Ca$_2$) and calcium-free (E2TG) forms of the Ca-ATPase?

The release of the structure of a calcium-free form of the Ca-ATPase (1iwo) has revealed large structural changes in the protein, accompanying the dissociation of calcium (Toyoshima and Nomura, 2002). In particular, movements in the cytoplasmic region to form a single headpiece as well as rearrangements of 6 of the 10 transmembrane helices have been evidenced. To identify the normal modes and thus the movements that contribute most to the transition (E1Ca$_2$ toward E2TG), the complete set of normal modes was projected on the normalized vector that describes the structural difference. This vector was constructed from the difference between the Cα atoms after optimal superimposition of the two x-ray structures (1eul and 1iwo). Fig. 8 shows the squared overlap (square dot product, plot *a*) and the cumulative squared overlap (plot *b*) of the modes with the difference vector. Twenty modes already account for 71% of the difference between the two structures and only 1000 modes are necessary to represent 98% of the difference. This shows that the low-frequency modes (large-amplitude movements) describe the difference between E1Ca$_2$ and E2TG, in agreement with the large structural changes observed (Toyoshima and Nomura, 2002).

Modes 7 and 8, the two slowest nonzero modes, have a contribution of 27.5% and 15.1%, respectively (Fig. 8 *a*). The next modes, 9–14, do not have major contributions whereas mode 15 contributes up to 13.3% to the difference vector. Thus, in total, three modes (7, 8, and 15) contribute for 55.9% to the difference vector. Modes 7 and 8 are characterized by large movements of the N domain whereas mode 15 shows movements of the lumenal loops, and in particular L7-8 (Figs. 2 and 3). Indeed, the two atomic structures show large rearrangements of the lumenal loops L7-8 and L3-4, becoming closer to each other. Interestingly, mode
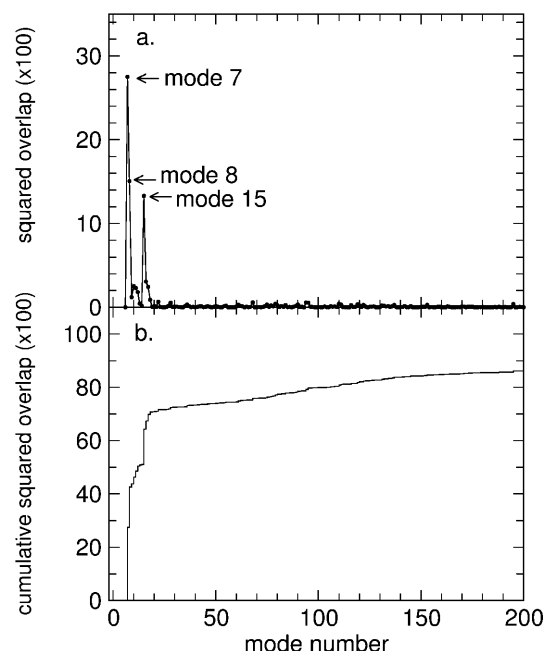

FIGURE 8 Squared overlap (*a*) and cumulative summation of the squared overlap (*b*) of the normal modes calculated on 1eul (E1Ca$_2$) and the difference vector between the Cα atoms of the 1eul (E1Ca$_2$) and 1iwo (E2TG) structures. Squared overlap ($\times$100) and cumulative squared overlap ($\times$100) are plotted against mode numbers (*x* axis restricted to modes 7–200).

9, characterized by a rotation of the M region and the N domain in opposite directions (Fig. 6), does not appear as a predominant mode in the E1Ca$_2$ toward E2TG transition (contribution equal to 1.2%). The same applies to modes 10–12 (contributions equal to 2.5%, 2.3%, and 1.8%, respectively), which describe the coupled movements of the A(+Nter) domain. The fact that those very slow modes, probably very important for the function of the pump, do not contribute to this calcium-binding transition may suggest that they are involved in other steps of the reaction cycle.

DISCUSSION

We have calculated the whole set of normal modes for the SERCA1 Ca-ATPase with a simplified method, requiring relatively modest computer resources but yielding results in good agreement with the experimental data. Because of their complexity, the movements undergone by the Ca-ATPase do not fall in any simple category of motion (hinge or shear) that occur in proteins (Echols et al., 2003). Through different analyses of the normal modes, we are able to describe a collection of movements and attempt to associate them with the different steps of the reaction cycle.

We have shown, by a thorough analysis of the first ten modes (7–16), the important mobility of N and A(+Nter) regions (Figs. 2 and 3). Among all putative movements of the protein that we describe, movements of both N and A(+Nter) domains are the ones with the largest amplitude,

i.e., N and A(+Nter) are the most displaced regions. This is in good agreement with the difference observed between the existing structures of the calcium pump in its E1Ca$_2$ (Toyoshima et al., 2000) and E2TG (Toyoshima and Nomura, 2002) or E2H$_3$-P-like (Xu et al., 2002) forms. Indeed one can easily observe that the cytoplasmic headpiece undergoes drastic changes (see Fig. 1). Moreover, we showed that these two regions behave as rigid bodies in the different movements: N and A, in their topological definition (Fig. 1), are dynamical domains (Fig. 4). Conversely, we demonstrated that P (N330–N359 and K605–D737) is a flexible region (Fig. 4 a), as is the stalk area, and can not be defined as a dynamical domain. A recent MD study (Costa and Carloni, 2003) also supports the hypothesis that P is flexible in the calcium-bound form of the pump. Toyoshima et al. suggested that the P domain, with flexible joints, functions as a coordinator of the transmembrane helices and also that the top part of M5 moves together with the P domain as a single entity. From our analysis, residues in P do not seem to undergo as large displacements as the N and A(+Nter) domains (Fig. 1). Neither could we find correlated movements of P and the top part of M4 or M5 in the low-frequency modes. Our calculations thus support the hypothesis that the signal transmission from the phosphorylation site to the M helices does not involve rigid-body motions of the P domain but rather small localized displacements and that the flexibility of this region is an advantage in transmitting those small displacements of P to the M5 helix and potentially along the M helices to the binding sites. However, even if the whole collection of normal modes can be calculated from one conformation, we can not exclude that normal modes of the phosphorylated form would show this type of movements of P whereas the nonphosphorylated form (used for these calculations) does not. To distinguish between the two possibilities, NMA of phosphorylated form is required; unfortunately this structure is not available.

The M region is a rigid region, but does not undergo large amplitude rigid-body motions (Figs. 2 and 3). We highlight a twist motion of the helices which does not seem to be correlated to P, but rather to the N domain (Fig. 6). We suggest that this movement is involved in the release of the calcium ions to the lumen. Indeed, in this movement, the lumenal extremity of the M domain (from the calcium binding sites to the lumenal loops) opens more than the top part, and the position of the backbone atoms of the residues involved in the calcium binding sites does not change significantly. In general, we found a much higher mobility of the lumenal loops than of the cytoplasmic loops (Fig. 2, c–e, and h–j). The observed mobility of the lumenal loops (L1-2, L3-4, L5-6, L7-8, and L9-10) is compatible with the existing structures and could explain the uptake/release of ions on the lumenal side. Interestingly, Toyoshima et al. report that the L3-4 loop comes closer to L7-8 (Toyoshima and Nomura, 2002). However, from our calculations, L7-8 appears to be more displaced than L3-4 in the slowest movements of the protein. Molecular modeling studies (Costa and Carloni, 2003; Li and Cui, 2002) also report the large mobility of the lumenal loops and suggest that L7-8 is more displaced than L3-4 (Costa and Carloni, 2003). The normalized atomic displacements associated with the cytoplasmic L6-7 loop, which is known to be functionally essential (Falson et al., 1997; Menguy et al., 1998), are not important, in any of the first 10 modes. This suggests that the movements of L6-7 are not large, which is in agreement with the molecular dynamics study of the E1Ca$_2$ form (Costa and Carloni, 2003). This is not in conflict with the functional role of L6-7 in calcium binding but simply implies that this role does not require large displacements of the loop.

The low-frequency modes highlighted only one concerted type of movement of the M helices. As this motion seems to open mostly the lumenal side of the M domain and very little the cytoplasmic side, it lead us to look for another type of movement to explain the cytoplasmic entrance of calcium. Investigation of the individual movements (rotation and translation) of the helices revealed interesting discrepancies in their ability to be displaced. The helices hosting the binding sites (M4, M5, M6, and M8) are less mobile than the other ones. Their inner position is probably one reason for that and the consequence for the stability of the calcium binding sites is obvious. Through molecular dynamics study of the calcium-bound form (Sites I and II occupied) and the forms with one (in Site I) or no calcium in the sites, Costa et al. (Costa and Carloni, 2003) reported recently that the orientation of helices M1–M3 is changed. Our findings illustrate the ability of those helices to be displaced; leading to the hypothesis that their mobility could play a role in the uptake of the calcium ions. Although directed mutagenesis has not shown any evidence for it, M1 has been suggested as an entry pathway for the calcium ions (Lee and East, 2001). Our calculations support this hypothesis since helices M1–M3 are more mobile than M4 and M6, which have been proposed as an alternative entrance pathway (Toyoshima et al., 2000).

NMA of the transition between the two available atomic structures (Fig. 8) has shown that only a few modes are involved in the transition between the Ca free (E2H$_3$) and bound (E1Ca$_2$) species. Modes 7, 8, and 15 describe the opening of the N domain as well as the movements of lumenal loops (Fig. 2) that are observed upon Ca binding (Toyoshima and Nomura, 2002). We looked further into the global calcium transport mechanism coupled to the ATP hydrolysis and tried to attribute the slow modes to the various steps of the catalytic cycle (Fig. 1). Indeed, as the E2TG→E1Ca$_2$ step, each transconformation occurring along the reaction cycle can be described by a combination of low-frequency modes. However, given the difference in the reactions occurring at each step of the catalytic cycle, it is expected that each transition will involve different modes of vibrations.

Modes 10 and 13 describe correlated movements of cytoplasmic domains that could contribute to the ATP binding and gamma phosphate transfer occurring within the phosphorylation step from $E1Ca_2$ to $E1Ca_2$-P.

Since it describes a concerted opening of the M helices at the lumenal side, the twist of the M helices described by mode 9 could be involved during the transition between $E1Ca_2$-P to $E2H_3$-P. Indeed, such a movement would facilitate the calcium release. Recently, Peinelt et al. (Peinelt and Apell, 2002) suggested that, during the $E1Ca_2$-P $\rightarrow$ $E2Ca_2$-P (low affinity binding sites) conformational change, either the binding sites are moved closer to the lumenal interface or a wide, water-filled vestibule is formed. The latter is totally in agreement with the observed mechanism of mode 9 where the helices twist open, motion that has also been recently reported (Li and Cui, 2002). One can easily imagine the same type of movement, in the opposite direction to twist close the lumenal side in the $E2H_3$-P $\rightarrow$ $E2H_3$ transition.

Several studies suggested an important role of the L7-8 loop in the Ca release pathway (Duggleby et al., 1999; Webb et al., 2000). Webb et al. (2000) suggested that the dephosphorylation step ($E2H_3$-P $\rightarrow$ $E2H_3$) involves movements of the lumenal loops. Indeed, chemical labeling of carboxyl groups on the lumenal side led to a loss in phosphorylation by P_i, suggesting an important role of the long acidic L7-8 loop. It was also suggested that calcium release involves structural rearrangements of the L7-8 loop (Duggleby et al., 1999). Our results support the hypothesis of the functional role of this loop due to its mobility.

Protease mediated excision of the $MAATE^{243}$ sequence from the loop linking the A domain with M3 strongly reduces the $E1Ca_2$-P to $E2H_3$-P transition without modification of both calcium binding and ATP phosphorylation processes (Møller et al., 2002). Thus the calcium release to the lumen probably involves a movement of the A domain. Modes 10–13, and 16 describe rotation and translation-like movements of the A domain which could describe the $E1Ca_2$-P to $E2H_3$-P transition. Moreover, these modes do not participate in the calcium binding step (Fig. 8) and the movements of the A domain are correlated with movements of other parts of the protein (L7-8 loop, N domain). Movements of the N and A domains have been analyzed by proteolysis studies of the different intermediates of the catalytic cycle of the Ca-ATPase. It has been observed that the efficiency of the proteolysis changes with the Ca-ATPase conformation (Andersen and Jorgensen, 1985; Danko et al., 2001a,b; Møller et al., 2002; Torok et al., 1988), suggesting a change in the accessibility of these sites. Limited digestion with trypsin shows that the first site (T1, Arg-505) located in a loop at the very top of the N domain of the Ca-ATPase is always accessible (Danko et al., 2001b). Nevertheless, the rate of degradation changes with the conformation and this could be correlated to the flexibility of this loop observed in several modes (Fig. 2). In particular, modes 14 and 16 show

a high mobility of this loop independently of the rest of the N domain (Fig. 2, *h* and *j*; Fig. 3 *f*). The second tryptic digestion site (T2, Arg-198) located in the A domain shows a more drastic change in accessibility since it becomes completely resistant to cleavage in the E2-P like form obtained in the presence of vanadate (Danko et al., 2001a,b). We do not believe that the difference between T1 and T2 is related to the amplitude of the displacement undergone by the A and N domains. It might instead be related to the position of the residues on the domain; T1 is placed at the very top of the N domain such that its accessibility will remain almost unchanged even if the cytoplasmic headpiece closes completely. Our calculation suggests that the A domain undergoes large movements that could be described by modes such as 10–13, and 16 (Fig. 2). Mode 11 in particular shows a large displacement of the loop containing the T2 site and the motion of A in this mode can be described as a translation of the domain along an axis almost perpendicular to the membrane plane.

In conclusion, our NMA of the slowest modes has enabled the description of large amplitude movements of the cytoplasmic domains of the Ca-ATPase. Comparison of the available atomic structure has shown the contribution of some of these slow modes to the transition between these structures. Analysis of the whole set of modes has also suggested the possible contribution of other modes, describing lower amplitude motions, in particular for the transmembrane helices. It opens a path toward analysis of the various movements of the Ca-ATPase occurring along the catalytic cycle.

REFERENCES

Abola, E., F. C. Bernstein, and S. H. Bryant, T.F. Koetzle, and J. Weng. 1987. Protein Data Bank. *In* Crystallographic Databases-Information Content, Software Systems, Scientific Applications. Data Commission of the International Union of Crystallography. Bonn. 107–132.

Andersen, J. P., and P. L. Jorgensen. 1985. Conformational states of sarcoplasmic reticulum Ca2+-ATPase as studied by proteolytic cleavage. *J. Membr. Biol.* 88:187–198.

Bahar, I., A. Atilgan, and B. Erman. 1997. Direct evaluation of thermal fluctuations in proteins using a single-parameter harmonic potential. *Fold. Des.* 2:173–181.

Bernstein, F. C., T. F. Koetzle, G. J. B. Willams, E. F. J. Meyer, M. D. Brice, J. R. Rodgers, O. Kennard, T. Shimanouchi, and M. Tasumi. 1977. The Protein Data Bank: A computer-based archival file for macromolecular structures. *J. Mol. Biol.* 112:535–542.

Brooks, B. R., R. E. Bruccoleri, B. D. Olafson, D. J. States, S. Swaminathan, and M. Karplus. 1983. CHARMM: a program for macromolecular energy, minimization, and dynamics calculations. *J. Comput. Chem.* 4:187–217.

Cornell, W., P. Cieplak, C. Bayly, I. Gould, K. M. Merz, D. Ferguson, D. Spellmeyer, T. Fox, J. Caldwell, and P. Kollman. 1995. A second generation force field for the simulation of proteins and nucleic acids. *J. Am. Chem. Soc.* 117:5179–5197.

Cornell, W. D., and S. Louise-May. 1998. Normal Mode Analysis. *In* Encyclopedia of Computational Chemistry. N.A. P. Schleyer, T. Clark, J. Gasteiger, P. Kollman, H. Schaefer, and P. Schreiner, editors. John Wiley & Sons. Chichester, UK. 1904–1913.

Costa, V., and P. Carloni. 2003. Calcium binding to the transmembrane domain of the sarcoplasmic reticulum Ca^{2+}-ATPase: Insights from molecular modeling. *Proteins.* 50:104–113.

Danko, S., K. Yamasaki, T. Daiho, H. Suzuki, and C. Toyoshima. 2001a. Organization of cytoplasmic domains of sarcoplasmic reticulum Ca(2+)-ATPase in E(1)P and E(1)ATP states: a limited proteolysis study. *FEBS Lett.* 505:129–135.

Danko, S., T. Daiho, K. Yamasaki, M. Kamidochi, H. Suzuki, and C. Toyoshima. 2001b. ADP-insensitive phosphoenzyme intermediate of sarcoplasmic reticulum Ca(2+)-ATPase has a compact conformation resistant to proteinase K, V8 protease and trypsin. *FEBS Lett.* 489:277–282.

Duggleby, R. C., M. East, and A. G. Lee. 1999. Luminal dissociation of $Ca2+$ from the phosphorylated Ca^{2+}-ATPase is sequential and gated by $Mg2+$. *Biochem. J.* 339:351–357.

Echols, N., D. Milburn, and M. Gerstein. 2003. MolMovDB: analysis and visualization of conformational change and structural flexibility. *Nucleic Acids Res.* 31:478–482.

Falson, P., T. Menguy, F. Corre, L. Bouneau, A. G. de Gracia, S. Soulie, F. Centeno, J. V. Moller, P. Champeil, and M. le Maire. 1997. The cytoplasmic loop between putative transmembrane segments 6 and 7 in sarcoplasmic reticulum Ca2+-ATPase binds Ca^{2+} and is functionally important. *J. Biol. Chem.* 272:17258–17262.

Forge, V., E. Mintz, and F. Guillain. 1993a. Ca^{2+} binding to sarcoplasmic reticulum ATPase revisited. I. Mechanism of affinity and cooperativity modulation by H^+ and Mg^{2+}. *J. Biol. Chem.* 268:10953–10960.

Forge, V., E. Mintz, and F. Guillain. 1993b. Ca^{2+} binding to sarcoplasmic reticulum ATPase revisited. II. Equilibrium and kinetic evidence for a two-route mechanism. *J. Biol. Chem.* 268:10961–10968.

Frishman, D., and P. Argos. 1995. Knowledge-based protein secondary structure assignment. *Proteins.* 23:566–579.

Go, N., T. Noguti, and T. Nishikawa. 1983. Dynamics of a small globular proteins in terms of low-frequency vibrational modes. *Proc. Natl. Acad. Sci. USA.* 80:3696–3700.

Green, N. M., and D. L. Stokes. 1992. Structural Modeling of P-type ion pumps. *Acta Physiol. Scand. Suppl.* 607:59–68.

Hayward, S. 2001. Normal mode analysis of biological molecules. *In* Computational Biochemistry and Biophysics. O.M. Becker, A.D. MacKerell, B. Roux, and M. Watanabe, editors. Marcel Dekker, Inc. New York. 153–168.

Hinsen, K. 1998. Analysis of domain motions by approximate normal mode calculations. *Proteins.* 33:417–429.

Hinsen, K. 2000. The molecular modeling toolkit: a new approach to molecular simulations. *J. Comput. Chem.* 21:79–85.

Hinsen, K., A. Thomas, and M. J. Field. 1999. Analysis of domain motions in large proteins. *Proteins.* 34:369–382.

Hinsen, K., A. Petrescu, S. Dellerue, M. Bellissent-Funel, and G. Kneller. 2000. Harmonicity in slow protein dynamics. *Chem. Phys.* 261:25–37.

Humphrey, W., A. Dalke, and K. Schulten. 1996. VMD- visual molecular dynamics. *J. Mol. Graph.* 14:33–38.

Lee, A. G., and J. M. East. 2001. What the structure of a calcium pump tells us about its mechanism. *Biochem. J.* 356:665–683.

Levitt, M., C. Sander, and P. S. Stern. 1985. Protein normal-mode dynamics: trypsin inhibitor, crambin, ribonuclease and lysozyme. *J. Mol. Biol.* 181:423–447.

Li, G., and Q. Cui. 2002. A coarsed-grained normal mode approach for macromolecules: an efficient implementation and application to Ca^{++}-ATPase. *Biophys. J.* 83:2457–2474.

Marques, O., and Y. Sanejouand. 1995. Hinge-bending motion in citrate synthase arising from normal mode calculations. *Proteins.* 23:557–560.

Menguy, T., F. Corre, L. Bouneau, S. Deschamps, J. V. Moller, P. Champeil, M. le Maire, and P. Falson. 1998. The cytoplasmic loop located between transmembrane segments 6 and 7 controls activation by Ca^{2+} of sarcoplasmic reticulum Ca^{2+}-ATPase. *J. Biol. Chem.* 273:20134–20143.

Møller, J. V., B. Jull, and M. Le Maire. 1996. Structural organization, ion transport, and energy transduction of P-type ATPases. *Biochim. Biophys. Acta.* 1286:1–51.

Møller, J. V., G. Lenoir, C. Marchand, C. Montigny, M. le Maire, C. Toyoshima, B. S. Juul, and P. Champeil. 2002. Calcium transport by sarcoplasmic reticulum Ca(2+)-ATPase. Role of the A domain and its C-terminal link with the transmembrane region. *J. Biol. Chem.* 277:38647–38659.

Mouawad, L., and D. Perahia. 1993. Diagonalization in a mixed basis: a method to compute normal-modes for large macromolecules. *Biopolymers.* 33:599–611.

Peinelt, C., and H. J. Apell. 2002. Kinetics of the Ca(2+), H(+), and Mg(2+) interaction with the ion-binding sites of the SR Ca-ATPase. *Biophys. J.* 82:170–181.

Reuter, N., K. Hinsen, and J. J. Lacapère. 2003a. The nature of the low-frequency normal modes of the E1Ca form of the SERCA1 Ca^{2+}-ATPase. *Ann. N. Y. Acad. Sci.* 986:344–346.

Reuter, N., K. Hinsen, and J. J. Lacapère. 2003b. Normal mode analysis of the Ca^{++}-ATPase based on a comparison between the E1Ca and E2TG structures. *Biophys. J.* 84:264a.

Schulz, G. E. 1991. Domain motions in proteins. *Curr. Opin. Struct. Biol.* 1:883–888.

Stokes, D. L., and N. M. Green. 2000. Modeling a dehalogenase fold into the 8-Å density map for Ca^{2+}-ATPase defines a new domain structure. *Biophys. J.* 78:1765–1776.

Stokes, D. L., and N. M. Green. 2003. Structure and function of the calcium pump. *Annu. Rev. Biophys. Biomol. Struct.* 32:445–468.

Tama, F., F. Gadea, O. Marques, and Y. Sanejouand. 2000. Building-block approach for determining low-frequency normal modes of macromolecules. *Proteins.* 41:1–7.

Thomas, A., K. Hinsen, M. J. Field, and D. Perahia. 1999. Tertiary and quaternary conformational changes in aspartate transcarbamylase: a normal mode study. *Proteins.* 34:96–112.

Tirion, M. 1996. Large amplitude elastic motions in proteins from a single-parameter, atomic analysis. *Phys. Rev. Lett.* 77:1905–1908.

Torok, K., B. J. Trinnaman, and N. M. Green. 1988. Tryptic cleavage inhibits but does not uncouple Ca^{2+}ATPase of sarcoplasmic reticulum. *Eur. J. Biochem.* 173:361–367.

Toyoshima, C., and H. Nomura. 2002. Structural changes in the calcium pump accompanying the dissociation of calcium. *Nature.* 418:605–611.

Toyoshima, C., H. Sasabe, and D. L. Stokes. 1993. Three-dimensional cryo-electron microscopy of the calcium ion pump in the sarcoplasmic reticulum membrane. *Nature.* 362:467–471.

Toyoshima, C., M. Nakasako, H. Nomura, and H. Ogawa. 2000. Crystal structure of the calcium pump of sarcoplasmic reticulum at 2.6 A resolution. *Nature.* 405:647–655.

Webb, R. J., Y. M. Khan, J. M. East, and A. G. Lee. 2000. The importance of carboxyl groups on the lumenal side of the membrane for the function of the Ca(2+)-ATPase of sarcoplasmic reticulum. *J. Biol. Chem.* 275:977–982.

Xu, C., W. J. Rice, W. He, and D. L. Stokes. 2002. A structural model for the catalytic cycle of Ca^{2+}-ATPase. *J. Mol. Biol.* 316:201–211.

Yu, X., S. Carroll, J. Rigaud, and G. Inesi. 1993. H^+ countertransport and electrogenicity of the sarcoplasmic reticulum Ca^{2+} pump in reconstituted proteoliposomes. *Biophys. J.* 64:1232–1242.

Zhang, P., C. Toyoshima, K. Yonekura, N. M. Green, and D. L. Stokes. 1998. Structure of the calcium pump from sarcoplasmic reticulum at 8-Å resolution. *Nature.* 392:835–839.